SANDIA REPORT
SAND2010-6429
Unlimited Release
Printed September 2010

Aerosol Cluster Impact and Break-up: II. Atomic and Cluster Scale Models

Jeremy B. Lechman and Yoichi Takato

Prepared by
Sandia National Laboratories
Albuquerque, New Mexico 87185 and Livermore, California 94550

Sandia National Laboratories is a multi-program laboratory managed and operated by Sandia Corporation, a wholly owned subsidiary of Lockheed Martin Corporation, for the U.S. Department of Energy's National Nuclear Security Administration under Contract DE-AC04-94AL85000.

Approved for public release; further dissemination unlimited.

Sandia National Laboratories

Issued by Sandia National Laboratories, operated for the United States Department of Energy by Sandia Corporation.

NOTICE: This report was prepared as an account of work sponsored by an agency of the United States Government. Neither the United States Government, nor any agency thereof, nor any of their employees, nor any of their contractors, subcontractors, or their employees, make any warranty, express or implied, or assume any legal liability or responsibility for the accuracy, completeness, or usefulness of any information, apparatus, product, or process disclosed, or represent that its use would not infringe privately owned rights. Reference herein to any specific commercial product, process, or service by trade name, trademark, manufacturer, or otherwise, does not necessarily constitute or imply its endorsement, recommendation, or favoring by the United States Government, any agency thereof, or any of their contractors or subcontractors. The views and opinions expressed herein do not necessarily state or reflect those of the United States Government, any agency thereof, or any of their contractors.

Printed in the United States of America. This report has been reproduced directly from the best available copy.

Available to DOE and DOE contractors from
U.S. Department of Energy
Office of Scientific and Technical Information
P.O. Box 62
Oak Ridge, TN 37831

Telephone: (865) 576-8401
Facsimile: (865) 576-5728
E-Mail: reports@adonis.osti.gov
Online ordering: http://www.osti.gov/bridge

Available to the public from
U.S. Department of Commerce
National Technical Information Service
5285 Port Royal Rd.
Springfield, VA 22161

Telephone: (800) 553-6847
Facsimile: (703) 605-6900
E-Mail: orders@ntis.fedworld.gov
Online order: http://www.ntis.gov/help/ordermethods.asp?loc=7-4-0#online

SAND2010-6429
Unlimited Release
Printed September 2010

Aerosol Cluster Impact and Break-up

Jeremy B. Lechman[1] and Yoichi Takato[2]
[1]Nanoscale and Reactive Processes Department
Sandia National Laboratories
P.O. Box 5800
Albuquerque, New Mexico 87185-MS0836
[2]Department of Physics
The State University of New York at Buffalo

Abstract

Understanding the interaction of aerosol particle clusters/flocs with surfaces is an area of interest for a number of processes in chemical, pharmaceutical, and powder manufacturing as well as in steam-tube rupture in nuclear power plants. Developing predictive capabilities for these applications involves coupled phenomena on multiple length and timescales from the process macroscopic scale (~1m) to the multi-cluster interaction scale (1mm – 0.1m) to the single cluster scale (~1000 - 10000 particles) to the particle scale (10nm – 10μm) interactions, and on down to the sub-particle, atomic scale interactions. The focus of this report is on the single cluster scale; although work directed toward developing better models of particle-particle interactions by considering sub-particle scale interactions and phenomena is also described. In particular, results of mesoscale (i.e., particle to single cluster scale) discrete element method (DEM) simulations for aerosol cluster impact with rigid walls are presented. The particle-particle interaction model is based on JKR adhesion theory and is implemented as an enhancement to the granular package in the LAMMPS code. The theory behind the model is outlined and preliminary results are shown. Additionally, as mentioned, results from atomistic classical molecular dynamics simulations are also described as a means of developing higher fidelity models of particle-particle interactions. Ultimately, the results from these and other studies at various scales must be collated to provide systems level models with accurate "sub-grid" information for design, analysis and control of the underlying systems' processes.

CONTENTS

1. Introduction 7

2. Mesoscale Model and Implentation 7
   2.1. JKR Particle Adhesion Model 7
   2.2. Model Implementation 10
   2.3. Sintered Particle Contact Constraint Model 13
   2.4. Enhancing Particle Interaction Models via Microscale (Atomistic) Simulations 13

3. Mesoscale Simulation Results 16
   3.1. Simulation Method 17
   3.2. Aerosol Cluster Formation 18
   3.3. Cluster-wall Impact 18

4. Conclusions and Future Work 20

5. References 20

Distribution 22

FIGURES

Figure 1. Normal force as a function of overlap, δ. Note: at contact, $\delta = 1.0$, force is non-zero due to adhesion while force for $\delta > 1.0$ applies only for separation after contact. 8
Figure 2. (a) Non-contact interparticle potential – equation (7) with ; (b) negative of interparticle force from potential in Equation (7). Lines same as in (a) except red line is negative of JKR force from equation (1). 9
Figure 3. Components of total energy during collision of particles of LJ atoms, $R = 11.4\sigma$ and $v_{coll} = 2.0\sqrt{\varepsilon/m}$: (a) total kinetic energy; (b) total potential energy; (c) temperature of particles 14
Figure 4. Coefficient of restitution for nanoparticle ($R = 11.4\sigma$) collisions as a function in impact velocity. Simulation snapshots indicate regimes of dissipative behavior 15
Figure 5. (a) Representative aerosol cluster formed by model cluster generator and (b) radius of gyration of cluster versus number of constituent particles... 17
Figure 6. Snapshots of the cluster from Figure 2 impacting a flat, rigid wall 18
Figure 7. Snapshots of the cluster from Figure 2 impacting a flat, rigid wall at moderate velocity (left) and high velocity (right) 19
Figure 8. Ejected cluster size distribution after collision with wall in terms of (a) fraction of total ejected clusters of a given size; and (b) close-up of small ejected clusters distribution, lines are guides to the eye 19

1. INTRODUCTION

Understanding particulate interactions and collective dynamics is of interest in a number of fields (e.g., soils, powder processing, colloidal suspensions, interstellar dust, etc.). In particular, particles are often small enough to be aerosolized. Often these particles form clusters of flocs as the agglomerate under the influence of long-range attractive interactions. The interaction of aerosolized clusters of particles with surfaces is vitally important to a number of applications including the potential dispersal of radioactive particles during steam-tube rupture in nuclear energy power plants. Numerical simulation has the potential to provide detailed information about the behavior of these particulate systems. Modeling the behavior of aerosol particles during agglomeration and cluster dynamics upon impact with a wall is of particular interest. Ultimately, this involves modeling a range of scales: from the multi-cluster interaction scale (1mm – 0.1m) to the single cluster scale (~1000 - 10000 particles) to the particle scale (10nm – 10μm) interactions, and on down to the sub-particle, atomic scale interactions. In this report we describe efforts to develop and implement physical models for aerosol particle-particle and particle-wall interactions. We focus on the cluster-wall interactions based on particle-scale models; but enhancing these models based on atomic information is also discussed.

Future work will consist of deploying these models to simulate aerosol cluster behavior upon impact with a rigid wall for the purpose of developing relationships for impact speed and probability of stick/bounce/break-up as well as to assess the distribution of cluster sizes if break-up occurs. These relationships will be developed consistent with the need for inputs into system-level codes. Section 2 gives background and details on the physical model as well as implementations issues and efforts to develop higher fidelity particle-particle interaction models. Section 3 presents some results of the particle-based (i.e., "mesoscale") simulations based on models discussed in Section 2. Section 4 presents several conclusions.

2. MESOSCALE MODEL AND IMPLENTATION

2.1. JKR Particle Adhesion Model

Following the work of Chokshi et al. [1] a number of researchers (e.g., [2-7]) have used particle-based techniques for investigating coagulation/agglomeration of small particles. What each of these has in common is that their physical models for the interaction of pairs of aerosol particles in the direction normal to the point of contact between the particles are derived from JKR theory [8]. JKR theory [8] combines Hertz's analysis of elastic deformation of contacting spheres with a constant attractive adhesive force when particles are in contact. The resulting equation for the magnitude of the normal force between contacting spheres of identical material and size is

$$F_n = \frac{8Ea^3}{3d(1-\nu^2)} - 2\pi a^2 \sqrt{\frac{2\gamma E}{\pi a(1-\nu^2)}} \tag{1}$$

where E is the Young's Modulus, ν is the Poisson ratio, γ is the surface energy per unit area, $d=2R$ is the diameter of the particle, and a is the radius of the contact circle between the spheres. The first term on the R.H.S. is the standard Hertz result. The second term is the force due to the surface adhesion of the particles. Equation (1) gives the relationship between the force and the contact circle radius for identical spheres; although the results can be generalized to convex particles of differing size and materials. Furthermore, the contact radius a can be related to the relative displacement δ as

$$\frac{\delta}{\delta_c} = 6^{1/3}\left[2\left(\frac{a}{a_0}\right)^2 - \frac{4}{3}\left(\frac{a}{a_0}\right)^{1/2}\right] \tag{2}$$

where the critical displacement at separation under tensile force is $\delta = -\delta_c$ with

$$\delta_c = \frac{2a_0^2}{d6^{1/3}} \tag{3}$$

and at equilibrium under zero applied force the contact circle radius

$$a_0 = \left(\frac{9\pi\gamma(1-\nu^2)d^2}{8E}\right)^{1/3} . \tag{4}$$

Note that for Hertzian contact without adhesion $\delta = 4a^2/d$. Equation (1) can be rewritten in a non-dimensional form as

$$\frac{F_n}{F_c} = 4\left[\left(\frac{a}{a_0}\right)^3 - \left(\frac{a}{a_0}\right)^{3/2}\right] \tag{5}$$

where $F_c=3\pi\gamma d/4$ is the force required to separate the adhered spheres. Figure 1 shows the value of the normal force as a function of the overlap, δ.

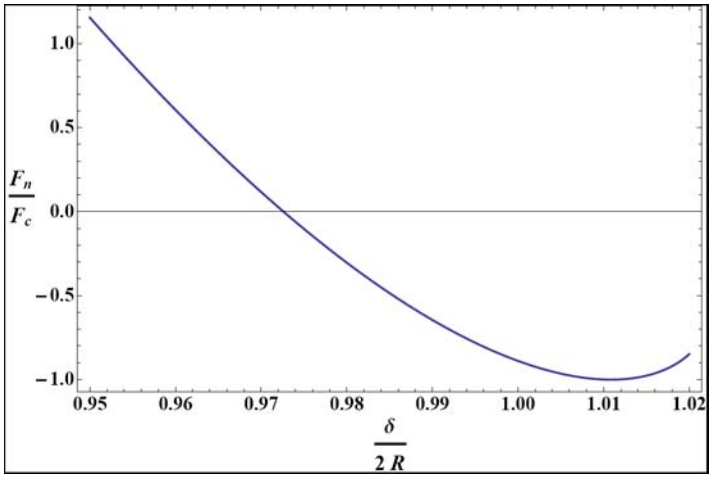

Figure 1: Normal force as a function of overlap, δ. Note: at contact, $\delta = 1.0$, force is non-zero due to adhesion while force for $\delta > 1.0$ applies only for separation after contact.

As noted above, many researchers seem to follow the work of Chokshi et al. in using the JKR theory of adhesion. However, alternatives have been proposed and debated in the literature most notably the DMT theory [9]. The differences between these were initially conceptual in formulating the problem, but led to very different predictions including different values of the pull-off force ($F_c=3\pi\gamma d/4$ for JKR and $F_c=\pi\gamma d$ for DMT). Later other approaches were developed to reconcile these discrepancies [10, 11]. From the later studies it was determined that JKR theory is appropriate for soft materials (i.e., low Young's Modulus) with high surface energies and large size whereas DMT theory is relevant for hard materials with low surface energies and small size; the key dimensionless parameter being

$$\kappa = \frac{32}{3\pi}\left(\frac{9d\gamma^2(1-\nu^2)^2}{2E^2 z_0^3}\right)^{1/3} = \frac{64}{3\pi}\left(\frac{d}{z_0}\right)\left(\frac{\gamma}{k_n}\right)^{2/3} \tag{6}$$

where z_0 is the separation at which the attraction between the sphere surfaces is maximum. At high κ, JKR applies and low κ, DMT. The second equality follows from the discussion below (see equation (7)). Tsai et al. [12] have raised objections to JKR, DMT and the "unified" MYD theories. In particular, a formulation which is consistent with long-range van der Waals attraction between macroscopic spheres may require formulating the problem along the lines of [12]; although it is not entirely clear that this is necessary.

In fact, it is difficult to reconcile the long-range attractive Van der Waals interactions with the surface energy adhesion energy without a detailed understanding of the nature of the short-range repulsive interactions (see z_0 in equation (6)) and surface structure and thermodynamics. The importance of the short-range repulsion can be seen if figure 2a where the potential

$$U(r_{ij}) = A\left[\exp(-(r_{ij}-r_0)/\sigma) - \frac{1}{6(r_{ij}-2R)}\right] \tag{7}$$

is plotted. Here, r_{ij} is the center-center particle separation, r_0 is the shift parameter, R is the radius of the particles (assumed equal sized), A is the Hamaker constant, and σ determines the range of the exponential repulsion (see z_0 in equation (6)). Alternatively, one could integrate the Lennard-Jones "12-6" atomistic potential to obtain the well know Hamaker attractive Van der Waals potential for macroscopic spheres and a repulsive term which has an analogous short-range repulsive lengthscale [21]. The difficulty with this approach is that the $1/r^{12}$ repulsive term in the LJ potential has no physical basis, but is chosen for computational expedience being "strong enough" to model Born repulsion of electron shells. When this term is integrated it becomes "weaker" ($1/r^7$). However, this doesn't seem physical as the nature of the repulsion remains a quantum mechanical and sub-atomic. Hence we choose to model the short-range repulsion as just that – by an exponential term (as is often done in atomic systems) shifted to the surface of the particle. This allows for demonstrating the significance of the range of the repulsive term as it determines the depth of the potential well and the strength of the "non-contact" attractive force as seen in figure 2b. In figure 2b, the JKR force is also compared to that determined from the non-contact interparticle potential equation (7). As can be seen, depending on the range of the repulsive force the magnitude of the Van der Waals force near contact can be a significant fraction of the JKR adhesion force. Also, the reason for taking the repulsive force to be a shifted exponential form becomes apparent in figure 2b from the small range between the zero force equilibrium distance, the attractive force at contact, and the pull-off force at $d+\delta_c$.

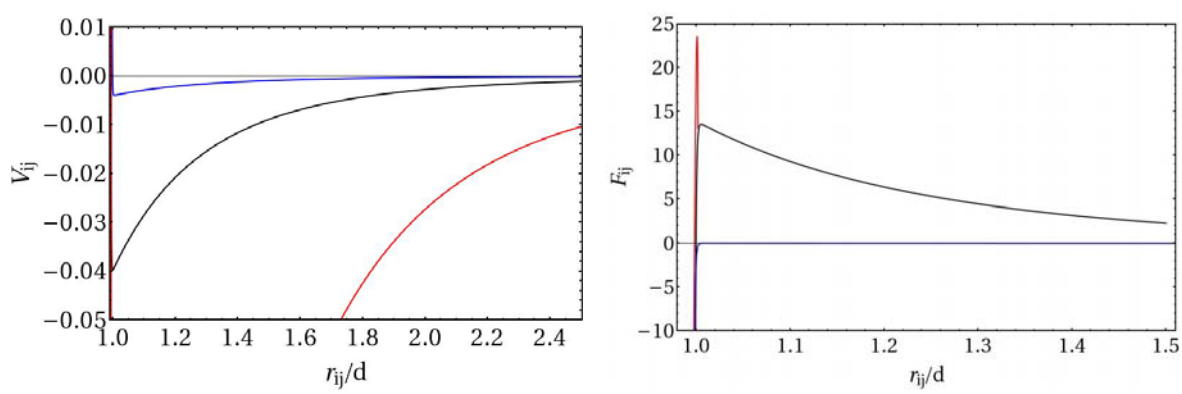

Figure 2: (a) Non-contact interparticle potential – equation (7) with ; (b) negative of interparticle force from potential in Equation (7). Lines same as in (a) except red line is negative of JKR force from equation (1).

Without further investigation into possible solutions to these issues, the JKR theory has been implemented as the particle-scale/mesoscale interaction model in the current work. Hence, materials with high κ are being simulated. Should it become necessary, a change to DMT would be trivial. Questions about compatibility with the Hamaker equation for long-range van der Waals attraction have been set aside initially since we neglect these interactions at present; although they can be included.

2.2. Model Implementation

The above model is easily implemented in Discrete Element Codes which allow for simulating the many particle dynamics of cluster formation and behavior upon impact. DEM is the large particle analog of Molecular Dynamics. Newton's equations of motion are solved for each individual discrete particle. The positions of all the particles are specified as the initial condition for the simulation. Then, using equations (2) and (3) the radius of the contact circle can be found for any pair of particles that are in contact. That is, delaying the discussion of tangential contact forces until later, for identical spheres *i* and *j* in contact, we note that $\delta = d - r_{ij}$ where $r_{ij} = |\mathbf{r}_i - \mathbf{r}_j|$. Having calculated δ for a pair of particles, solving equation (2) for a now allows us to find the force acting between the particles via equations (4) and (5). The forces on each particle are summed and Netwon's First Law is integrated to get the velocities and integrated again to get the displacement. This is done for each particle. The particles are then moved and the new configuration allows us to repeat the process thereby iteratively evolving of the multi-particle dynamics.

Accordingly, equations (2-5) form the basis of the adhesive particle model implemented in Sandia's Large Atomic-Molecular Massively Parallel Simulator (LAMMPS) code. The current LAMMPS implementation of adhesive particle models is similar to previous work [5]; however a few differences in the details should be pointed out. As part of the general distribution, LAMMPS contains a "Granular" package that allows one to perform particle simulations using the Discrete Element Method (DEM) [13]. LAMMPS's basic granular model for grain-grain interactions is based on the visco-elastic contact forces derived in [14]. These include a normal Hertzian elastic and a dissipative force describing the inelasticity of real materials; although the exact atomistic nature of the dissipative force remains an open subject. Note the dissipative force does not appear in equations (1) or (5). The tangential frictional forces are represented similarly using a Mindlin-type model [15]. In practice this amounts to a spring and a dashpot model for both the normal and tangential contact forces with the addition of a slider in the tangential model due to the Coulomb friction limit. To this basic model were added additional terms representing the surface adhesive force at contact as well as other terms, which restrict relative translation, rotation and twisting.

In the basic LAMMPS granular model, the user specified parameters for the normal interactions are the normal stiffness (with units of force/distance)

$$k_n = \frac{Ed}{3(1-\nu^2)} \tag{7}$$

and damping coefficient (with units of mass/time)

$$\eta_n = \frac{1}{3}\frac{(3\lambda-\zeta)^2}{(3\lambda+2\zeta)}\left[\frac{(1-2\nu)}{2\nu^2}\right]\sqrt{d\delta} \tag{8}$$

where ν is Poisson's ratio and ζ and λ are the shear and bulk "viscosities", respectively, of the material. **Note we have again assumed equal sized spheres of identical materials.** In the model of [5] following [15] the normal damping coefficient is written as

$$\eta_n = \alpha\left[2mk_n\right]^{1/2}\left(\frac{\delta}{d}\right)^{1/4} \tag{9}$$

with m the mass of the particle. Equation (9) is derived heuristically with the empirical coefficient α related to the coefficient of restitution. The visco-elastic model underlying equation (8) by contrast allows the damping coefficient to be specified independent of the normal stiffness – at least there is no explicit dependence on the normal stiffness even though there is an implicit dependence through the relative normal displacement δ. Similarly, the user specified parameters for the tangential interactions are the coefficient of friction

$$\mu \le \frac{F_t}{F_n} \tag{10}$$

where F_n and F_t are the normal and tangential force magnitudes, respectively. The tangential stiffness is defined by

$$k_t = \frac{E}{(2-\nu)(1+\nu)}\sqrt{d\delta} = \frac{2G}{2-\nu}\sqrt{d\delta} \tag{11}$$

where G is the shear modulus. Equation (11) is based on the analysis of Mindlin and Deresiecz for the case of no-slip [15]. Implied by equation (11) is the fact that the tangential force-displacement relationship depends on the relative normal displacement. Finally, and tangential damping coefficient can also be specified; however it has been ignored (i.e., set equal to zero) in the current work.

Given the above discussion, the magnitude of the total normal force acting on particles i and j in contact, again assuming identical particles, can be written as

$$\frac{F_{n,ij}}{F_c} = 4\left[\left(\frac{a}{a_0}\right)^3 - \left(\frac{a}{a_0}\right)^{3/2}\right] - \frac{4\eta_n}{3\pi\gamma d}(\mathbf{v}_{ij}\cdot\mathbf{n}_{ij}) \tag{12}$$

where $\delta(a)$ is given in equation (2) and $\mathbf{v}_{ij} = |\mathbf{v}_i - \mathbf{v}_j|$ is the relative velocity of the pair and $\mathbf{n}_{ij}$ the unit normal vector and the contact. The magnitude of the tangential force is given by

$$\frac{F_{t,ij}}{F_c} = \frac{4k_t\delta}{3\pi\gamma d} \tag{13}$$

where k_t is defined in equation (11) and the tangential force is limited by the adhesion analog of equation (10), namely

$$F_{t,ij} \le \mu(F_{n,ij} + 2F_c). \tag{14}$$

Note it is more convenient to write the tangential force in terms of δ and not a as in equation (12). Recall that δ is the quantity calculated directly during the force determination; subsequently equation (2) is solved for a and used in (12). In fact, equation (2) is solved analytically (selecting the root that gives real values) and implemented in the code. The total force on particle i can now be written as

$$\mathbf{F}_i = \sum_{j \ne i} F_{n,ij}\mathbf{n} + F_{t,ij}\mathbf{t} \tag{15}$$

where **t** is the unit vector tangential to the contact and in the direction of sliding (**n** x **t** = *0*). Additional forces including long-range van der Walls attraction or electrostatic repulsion (i.e., DLVO-type forces) and forces due to particle-fluid interactions (Brownian, drag, etc.) are available in LAMMPS or by coupling LAMMPS to a fluid flow solver and can be included at a later date.

2.3. Adhered Particle Contact Constraint Model

In addition to the JKR adhesion which applies to the forces between particle pairs in contact, a model for sintered constraints between contacting particles has been implemented. In addition to the tangential and normal forces a torque between contacting particles is included. This model follows [5] and details can be found there. Here we outline some of its aspects in the LAMMPS implementation. The total torque on a particle i is given by

$$T_i = \sum_{j \ne i} RF_{n,ij}(\mathbf{n} \times \mathbf{t}) + T_{r,ij}(\mathbf{t}_r \times \mathbf{n}) + T_{t,ij}\mathbf{n} \tag{16}$$

where $\mathbf{t}_r$ is the unit vector tangential to the contact and in the direction of rolling, T_r is magnitude of the torque on the particle due to the rolling resistance and T_t is the magnitude of the torque due to resistance twisting of the particle about the contact normal. As mentioned, further details can be found in [5]. The twisting torque is limited by

$$M_t \le -\frac{2}{3}\mu a(F_n + 2F_c) \tag{17}$$

while the rolling torque satisfies

$$\boldsymbol{M_r \leq k_r \xi_{crit}} \tag{18}$$

where $k_r = 4F_c(a/a_0)^{3/2}$ is the rolling "stiffness" and ξ_{crit} is the is the critical rolling displacement [5] which is a user specified value. This sintered particle model can be used in conjunction with the JKR adhesion or the user can choose to perform simulations with JKR adhesion only.

2.4. Enhancing Particle Interaction Models via Microscale (Atomistic) Simulations

As noted above, a number of outstanding questions remain for connecting the particle-level inter-particle interactions with a detailed atomistic approach. In particular, while most mesoscale inter-particle force models include a viscous damping term (see equations (8), (9), and (12)) to dissipate energy the actual nature of the dissipation mechanisms being modeled in particle collisions are not well understood. Additionally, as noted previously, the connection between the longrange, noncontact Van der Waals attraction, adhesion due to surface energy effects and the constraints (sliding, rolling, twisting) induced, and particle surface structure remain poorly characterized. These phenomena play a crucial roll in developing better models of particle-particle collisions leading to sticking, bouncing, fracture, etc. Many have sought to predict these phenomena by considering energy balance at the particle scale [22,23,24]. Therefore, to elucidate these mechanisms we perform atomistic classical molecular dynamics simulations of colliding particles of nanometric dimension. Initially we have focused on the nature of the dissipation mechanisms in collisions of purely repulsive particles.

The nano-sized particles considered here are roughly spheres of various radii, R constructed from a face-centered cubic (fcc) lattice of Lennard-Jones atoms. We simulated different sizes of nano-particles ranging from $R = 6.5\sigma$ to $R = 29.4\sigma$. As noted, the particles are not perfect spheres; there exist faceted faces on the particles due to the underlying fcc lattice of atoms. To simulate collisions, two identical particles are placed with facets facing each other (see figure 3) and they are given equal and opposite center-of-mass velocities. We use classical MD for this study and consider nanocluster constituent atoms whose potential is expressed by Lennard-Jones (L-J) potential:

$$U(r_{ij}) = \begin{cases} 4\varepsilon\left(\left(\dfrac{\sigma}{r_{ij}}\right)^{12} - \left(\dfrac{\sigma}{r_{ij}}\right)^{6}\right), & r_{ij} \leq r_{cut} \\ 0 & r_{ij} > r_{cut} \end{cases} \tag{19}$$

where r_{ij} is an inter-atomic distance between atoms i and j, and r_{cut} is a cut-off distance. We set $r_{cut} = 2.5\sigma$ for atoms interacting within a single particle, which is typically used for the L-J potential. In addition, we ignore cluster-cluster adhesive interactions, and therefore, we set $r_{cut} = 2^{1/6}\sigma$ (purely repulsive) for interactions between atoms belonging to different clusters. Note that the units used here are the standard non-dimensional LJ units, i.e., the unit for energy ε, distance

σ, and the unit for mass m. In addition to these units, the "derived" units for velocity $\sqrt{\varepsilon/m}$, temperature ε/k_B, where k_B is Boltzmann constant, and time $\tau = (m\sigma^2/\varepsilon)^{1/2}$ are used.

The full simulation procedure follows a number of steps. First, two identical clusters are placed and thermally equilibrated over 10,000 MD steps, controlling temperature $T = 0.02\varepsilon/k_B$ using the Nose-Hoover thermostat. After reaching an equilibrium state, the clusters are given equal and opposite center-of-mass velocities and are thus set to collide with a relative collision velocity of v_{coll}. The collision process is carried out in the microcanonical ensemble (NVE). For most system sizes, v_{coll} is varied from $0.03\sqrt{\varepsilon/m}$ to $3.3\sqrt{\varepsilon/m}$. The time step is set to be $\Delta t = 0.005\tau$ for all cases. The relative residue of the total energy of a system during calculations is conserved around 10^{-5}. This is achieved for finite cutoffs by shifting the potential to zero at r_{cut}. In order to quantify errors in calculated quantities, we perform multiple simulations for each collision velocity by setting different initial thermal velocities.

Figure 3 shows sample results for the various components of the total energy of colliding nanoparticles ($vcoll = 2.0\sigma/\tau$, $R = 11.4\sigma$). Two features stand out. First, due to the NVE ensemble the temperature of the particles increases which allows for "softening" due to melting of the FCC structure. Secondly, large deformation of the particle is expected as indicated by the change in total potential energy. This later difference should be related to the energy of cold work and an important component in the development of a thermo-mechanical model of particle-particle impact.

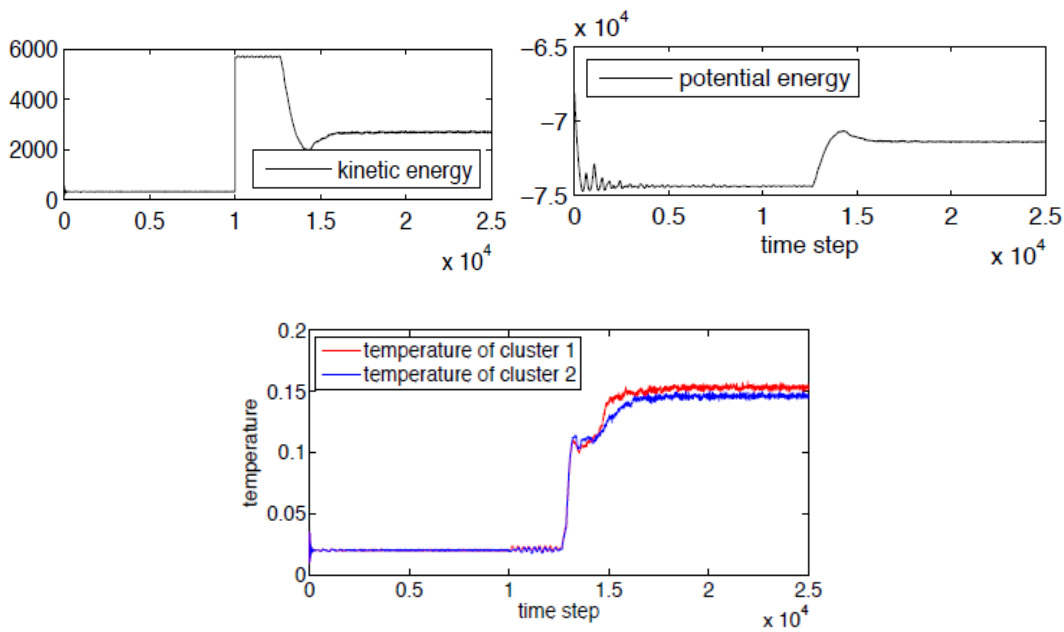

Figure 3: Components of total energy during collision of particles of LJ atoms, $R = 11.4\sigma$ and $v_{coll} = 2.0\sqrt{\varepsilon/m}$: (a) total kinetic energy; (b) total potential energy; (c) temperature of particles.

The simplest way to demonstrate the various dissipation mechanisms is in terms of the well know coefficient of restitution for colliding particles. From data given in the energy budget a coefficient of restitution can be calculated according to

$$e = \sqrt{1 - \frac{\Delta E_{therm} + \Delta E_{pot}}{K_{cm}}} \tag{20}$$

where ΔE_{thrm} and ΔE_{pot} are the thermal and potential energy changes respectively and K_{cm} is the initial center-of-mass kinetic energy. The coefficient of restitution is plotted in figure 4 as a function of v_{coll}. Several regimes of particle behavior can be seen. At low impact velocity the collision is elastic ($e \approx 1$). At $v_{coll} \approx 0.4\sqrt{\varepsilon/m}$ a transition takes place and increasing the impact velocity decreases e. As can be seen in the snapshots of the particles, this is due to increasing deformation of the particles. Initially this deformation takes the form of dislocations along particular directions. Increasing v_{coll} leads to increased plastic deformation. At large v_{coll} (> ~ $2.0\sqrt{\varepsilon/m}$) the increased temperature allows for weakening of the FCC solid so that very large plastic flow can take place.

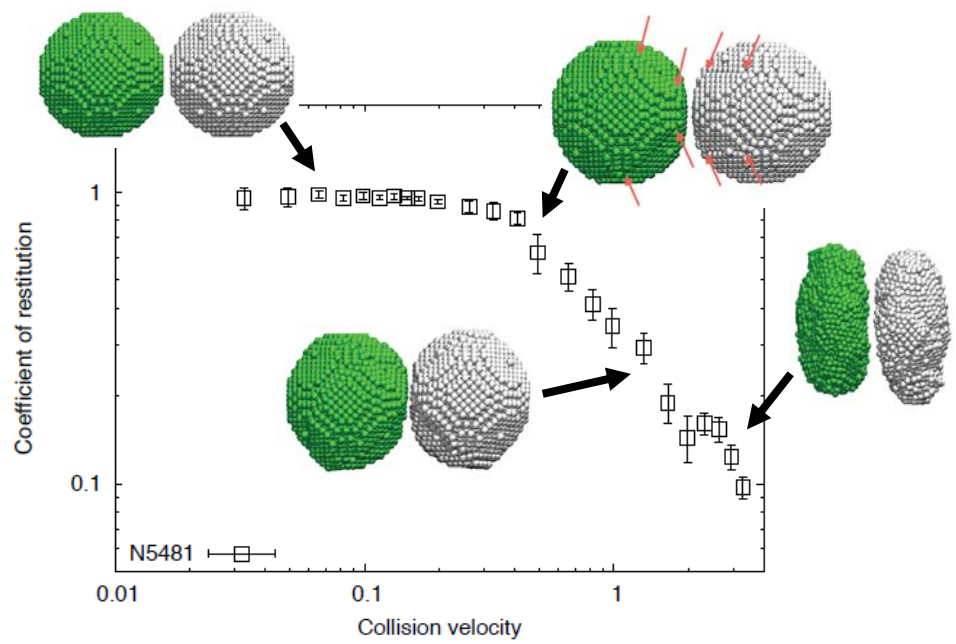

Figure 4: Coefficient of restitution for nanoparticle ($R = 11.4\sigma$) collisions as a function in impact velocity. Simulation snapshots indicate regimes of dissipative behavior.

From these results models of dissipation at the particle scale can be derived. Additionally, allowing inter-particle attraction and changing the particle composition will allow to explore dissipation mechanism and attractive interactions in a broader class of systems.

3. MESOSCALE SIMULATION RESULTS

In this section, the mesoscale simulation setup and methods are described as well as results.

3.1. Simulation Method

DEM simulations to study aerosol cluster impact and break-up were performed. Identical spherical particles are the constituents of the clusters. Initially, gravity, long-range (i.e., non-contact) Van der Waals attraction and electrostatic repulsion between particles and the wall, and interaction with a background fluid have been ignored. In order to perform the simulations the following steps were taken:

- Generate initial fractal clusters
  - Build directly with target fractal dimension ~2.0 (ballistic cluster-cluster aggregation-like models – BCCA)
- "Throw" clusters at flat, rigid wall varying impact velocity
  - Initially ignore fluid flow and particle-fluid coupling
  - Initially assume no random motion of particles, which may occur due to thermal, or turbulent fluctuations in the background fluid
- Characterize agglomerate response: fracture probability and fragment size distribution, etc.
- Develop models to predict response based on agglomerate characteristics and impact conditions

In performing the simulations the flowing non-dimensional units were used

- Length: $d = 1.0$
- Mass: $m = 1.0$
- Time: $\tau = \sqrt{d/g}$, where g is the acceleration of gravity, representing the time taken for a particle to fall its own diameter under the influence of gravity ($g = 1.0$ in non-dimensional units)
- Force: γd
- Energy: γd^2

A key dimensionless ratio is γ/k_n as can be seen by substituting equations (4) and (7) into equation (12) (see also equation (6) and the discussion concerning it). It should be noted at this point that although we have a direct relationship between elastic material properties of a material and k_n (equation (7)), for computational efficiency for very stiff materials (e.g., glass) the value of k_n used in the simulations is several orders of magnitude smaller than the value determined by equation (7). This is due to the stability of the time-stepping scheme where the timestep must satisfy $\delta t < \sqrt{m/k_n}$. Hence the larger k_n the smaller δt. Realizing this requires γ to be adjusted accordingly in the simulation while keeping the ratio γ/k_n equivalent to the physical value. Another key ratio for particle-particle (similar for particle-wall) collisions is

$$\lambda = \frac{2F_c\delta_c}{mv_0^2} = \frac{(3\pi)^{5/3}}{4*6^{1/3}}\left(\frac{\gamma}{k_n}\right)^{2/3}\left(\frac{\gamma d^2}{mv_0^2}\right) = \frac{(3\pi)^{5/3}}{4*6^{1/3}}\left(\frac{1}{c}\right)\left(\frac{\gamma}{k_n}\right)^{5/3} \quad (21)$$

where v_0 is the initial velocity of the particle (i.e., velocity prior to impact) and c is a constant related to converting the time units in the velocity to $\sqrt{m/k_n}$ which, according to the above,

originally had units of $\tau = \sqrt{d/g}$. Equation (21) is the ratio of adhesion energy to kinetic energy for a single particle. The value of this ratio is related to whether colliding particles will stick or not (ignoring inelastic dissipation in the collision) [1]. This ratio indicates that if γ is to be scaled while keeping the ratio γ/k_n constant then the velocity must be scaled as well to recover the correct stick or bounce behavior of the particle-particle (particle-wall) interaction.

3.2. Aerosol Cluster Formation

The initial conditions for a simulation of an aerosol cluster impacting a wall consists of specifying the geometry of the cluster. It is well known that the fractal dimension of the cluster describing its geometry depends on the agglomeration process [16, 17]. A couple approaches can be taken to build these initial fractal clusters. One can either simulate the exact formation process [e.g., 19, 20], or the clusters can be built by an algorithm which attempts to model the physical formation process [e.g., 18, cf. 6 and 7]. Since the former can be algorithmically and computationally intensive, the latter process will be adopted. Figure 5a shows a representative cluster of 4096 particles generated from an algorithm similar to [18]. Figure 5b shows the method for determining the fractal dimension from the scaling of the radius of gyration with number of constituent particles in the cluster. This algorithm yields clusters with fractal dimensions ~2.05. Modifications can be made to yield fractal dimensions ~1.91 [18]. Alternative algorithms can give clusters of arbitrary fractal dimensions. One hundred random clusters were built with this cluster and simulated to determine the statistical results of cluster-wall collisions.

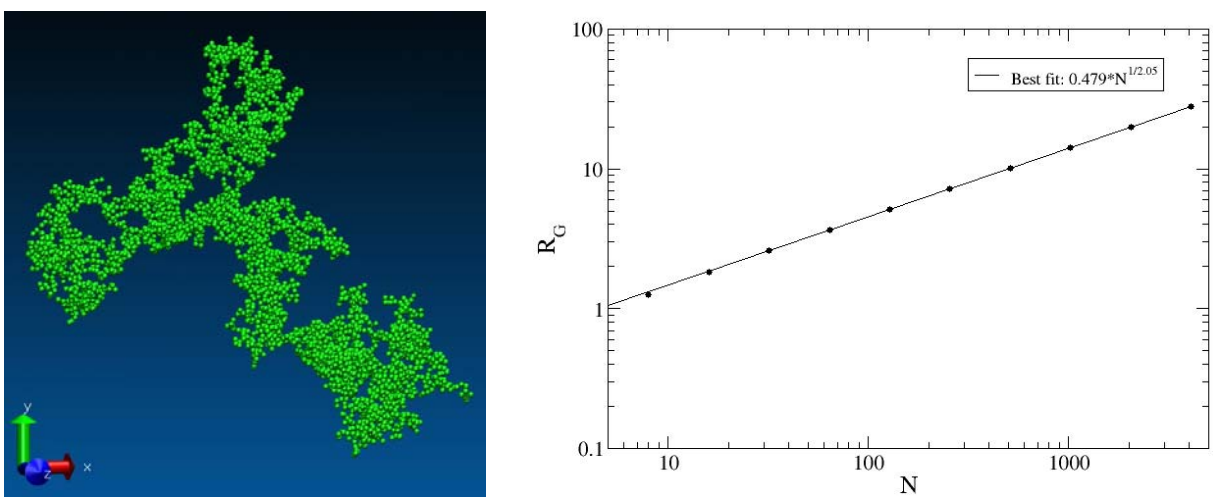

(a) **(b)**

Figure 5: (a) Representative aerosol cluster formed by model cluster generator and (b) radius of gyration of cluster versus number of constituent particles (4096 total constituent particles).

3.3. Cluster-wall Impact

Taking the cluster of figure 5, one can "throw" it against a flat, rigid wall and observe the behavior as in figures 6. The parameters for this simulation were $\gamma/k_n = 5x10^{-5}$, $\eta_n = 50$, $\mu = 0.5$ the initial impact velocity of the cluster was $0.1d/\tau$. The timestep $\Delta t = 1x10^{-6}\tau$ and the simulations were run for $2500000\ \Delta t$, well past the collision with the wall in all cases. There was no attractive interaction between the wall and the individual particles, but the Hertzian elastic and frictional interactions are the same between the grain-grain and grain-wall interactions. Although the snapshots end before rebound of the cluster from the wall impact, it can be seen that these parameters give a very ductile-like response with no cluster fracture/break-up.

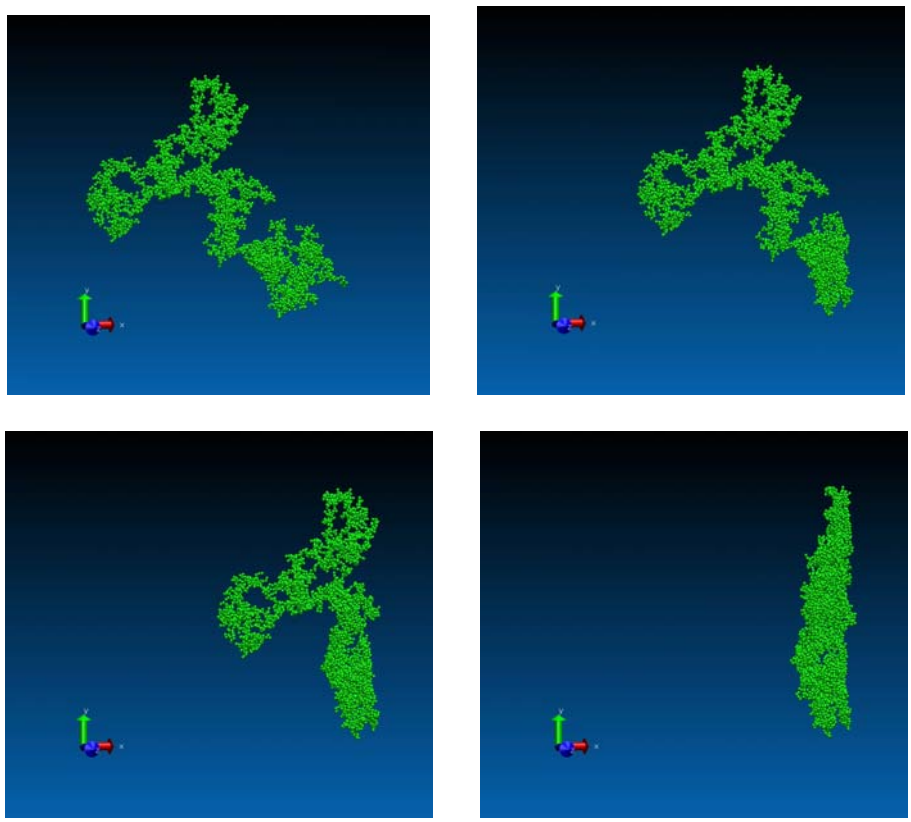

Figure 6: Snapshots of the cluster from Figure 2 impacting a flat, rigid wall.

In contrast to low impact velocity collisions, figure 7 shows snapshots of moderate, $1.0d/\tau$ (left), and very high, $100d/\tau$ (right), impact velocities. As can be seen, moderate impact velocities lead to cluster break-up into a number of smaller, ejected clusters of varying size while higher impact velocities can lead to nearly complete disintegration of the cluster.

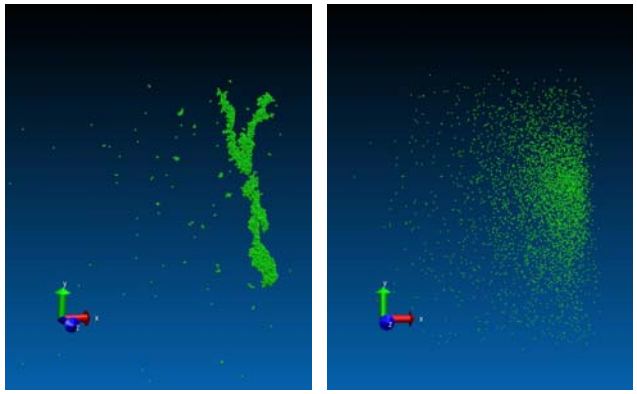

Figure 7: Snapshots of the cluster from Figure 2 impacting a flat, rigid wall at moderate velocity (left) and high velocity (right).

To quantify these observations we perform 100 identical simulations of different randomly generated clusters of 4096 particles and fractal dimension of ~2.05. Figure 8 shows the results of these simulations plotted as the average fraction of ejected clusters of a given size versus cluster size. The average is taken over the 100 simulations for each impact velocity. The error bars represent the standard deviation of the fraction of clusters of a given size in the sample of 100 simulations. For moderate and lower impact velocities the error bars large and many more simulations must be run to determine whether the same trend as in the small cluster size distribution continues. Clearly, as the impact velocity increases the vast majority of ejected clusters are single particles.

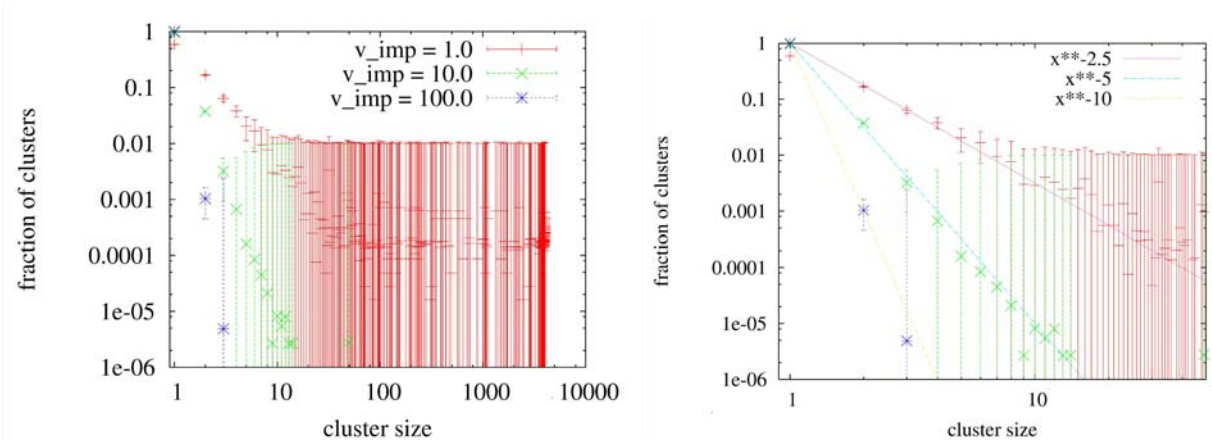

Figure 8: Ejected cluster size distribution after collision with wall in terms of (a) fraction of total ejected clusters of a given size; and (b) close-up of small ejected clusters distribution, lines are guides to the eye.

Based on the results in figure 8, it can be seen that the majority of ejected clusters are of small size (< ~50 particles), e.g., 1 in ~10000 ejected clusters has less than 50 particles for $v_{imp} = 1.0\ d/\tau$ and fewer for higher impact velocities. Although more simulations must be run at moderate and lower impact velocities to reduce the uncertainties in the results, it seems that smaller ejected cluster sizes have a clear power law behavior. Therefore, ignoring larger cluster sizes and

recognizing the slight over-prediction of smallest cluster sizes for moderate impact velocities, we can tentatively propose an empirical scaling relation for use systems levels models as follows

$$P(N_i) \sim N_i^{-\alpha} \tag{22}$$

That is, the probability of a given ejected cluster size follows a power law in the ejected cluster size. Note a normalization constant remains undetermined in (22) and care should be taken to find it particularly since (22) slightly over-estimates the smallest ejected cluster sizes for the moderate impact velocities. From figure 8b an interesting result is suggested for the dependence of the exponent in (22) on the impact velocity.

$$\alpha \sim v_{imp}^{0.3} \tag{23}$$

Again the normalization constant remains undetermined. Practically, if this empirical scaling relation holds this constant would be determined by the value of α at the onset of cluster break-up. Here it can be taken to be 2.5 giving $\alpha = 2.5$ at collision velocity of $1d/\tau$.

4. CONCLUSIONS AND FUTURE WORK

Physical models for aerosol particle dynamics and adhesion have been implemented in Sandia National Laboratories' Large Atomic Molecular Massively Parallel Simulator. Both sub-particle, atomic level simulations and mesocale, particle-scale simulations have been performed. Initial results of atomic simulation provide promise that higher fidelity particle-particle interaction models can be developed, particularly with regard to dissipation mechanisms. Results from the mesoscale simulations indicate that this technique can be useful in developing scaling relationships for ejected cluster size distribution in floc-wall collision studies. These models may prove useful in systems level codes where modeling of individual particles is too computationally intensive.

5. REFERENCES

1. Chokshi, A., A. G. G. M. Tielens, and D. Hollenbach, *Dust Coagulation*, The Astorphysical Journal, 407:806-819, 1993.
2. Dominik, C. and A. G. G. M. Tielens, *The Physics of Dust Coagulation and the Structure of Dust Aggregates in Space*, The Astrophysical Journal, 480:647-673, 1997.
3. Marshall, J. S., *Particle Aggregation and Capture by Walls in a Particulate Aerosol Channel Flow*, Journal of Aerosol Science, 38:333-351, 2007.
4. Li, S.-Q. and J. S. Marshall, *Discrete Element Simulation of Micro-particle Deposition on a Cylindrical Fiber in an Array*, Journal of Aerosol Science, 38:1031-1046, 2007.
5. Zhao, Y. and J. S. Marshall, Spin *Coating of a Colloidal Suspension*, Physics of Fluids, 20:043302-1-15, 2008.
6. Wada, K., H. Tanaka, T. Suyama, H. Kimura, and T. Yamamoto, *Numerical Simulation of Dust Aggregation Collisions. I. Compression and Disruption of Two-dimensional Aggregates*, The Astrophysical Journal, 661:320-333, 2007.

7. Wada, K., H. Tanaka, T. Suyama, H. Kimura, and T. Yamamoto, *Numerical Simulation of Dust Aggregation Collisions. II. Compression and Disruption of Three-dimensional Aggregates in Head-on Collisions*, The Astrophysical Journal, 667:1296-1308, 2008.
8. Johnson, K. L., K. Kendall, and A. D. Roberts, *Surface Energy and the Contact of Elastic Solids*, Proceedings of the Royal Society of London A, 324:301-313, 1971.
9. Derjaguin, B. V., V. M. Muller, and YU. P. Toporov, *Effect of Contact Deformation and the Adhesion of Particles*, Journal of Colloid and Interface Science, 53:314-326.
10. Muller, V. M., V. S. Yushchenko, and B. V. Deraguin, *On the Influence of Molecular Forces on the Deformation of an Elastic Sphere and Its Sticking to a Rigid Plane*, Journal of Colloid and Interface Science, 77:91-101, 1980.
11. Muller, V. M., V. S. Yushchenko, and B. V. Deraguin, *General Theoretical Consideration of the Influence of Surface Forces on the Contact Deformations and the Reciprocal Adhesion of Elastic Spherical Particles*, Journal of Colloid and Interface Science, 92:92-101, 1983.
12. Tsai, C.-J., D. Y. H. Pui, and B. Y. H. Liu, *Elastic Flattening and Particle Adhesion*, Aerosol Science and Technology, 15:239-255, 1991.
13. Silbert, L., D. Ertaş, G. S. Grest, T. C. Halsey, D. Levine, and S. J. Plimpton, *Granular Flow Down an Inclined Plane: Bagnold Scaling and Rheology*, Physical Review E, 64:051302-1-14, 2001.
14. Brilliantov, N., F. Spahn, J.-M. Hertzsch, and T. Pöschel, *Model for Collisions in Granular Gases*, Physical Review E, 53:5382-5392, 1996.
15. Tsuji, Y., T. Tanaka, and T. Ishida, *Lagrangian Numerical Simulation of Plug Flow of Cohesionless Particles in a Horizontal Pipe*, Powder Technology, 71:239-250, 1992.
16. Meakin, P., *Fractal Aggregates in Geophysics*, Reviews of Geophysics, 29:317-354, 1991.
17. Witten, T. A. and M. E. Cates, *Tenuous Structures from Disorderly Growth Processes*, Science, 1607-1612, June 27, 1986.
18. Jullien, R., *Transparency Effects in Cluster-Cluster Aggregation with Liner Trajectories*, Journal of Physics A: Mathematical and General, 17:L771-L776, 1984.
19. Kempf, S., S. Pfalzner, and T. K. Henning, *N-particle-simulations of Dust Growth I. Growth Driven by Brownian Motion*, Icarus, 141:388-398, 1999.
20. Kempf, S. and S. Pfalzner, *An Effective Algorithm for Simulating Diffusion-driven Aggregation*. Computer Physics Communications, 137:225-235, 2001.
21. Everaers, R. and Ejtehadi, M. R., *Interaction Potentials for Soft and Hard Ellipsoids*. Physical Review E, 67:041710, 2003.
22. Dahneke, B., *The Capture of Aerosol Particles by Surfaces*. Journal of Colloid and Interface Science, 37:342-352, 1971.
23. Dahneke, B., *Particle Bounce or Capture – Search for and Adequate Theory: I Conservation-of-Energy for a Simple Collision Process*. Aerosol Science and Technology, 23:25-39, 1995.
24. Andres, R. P., *Inelastic Energy Transfer in Particle/Surface Collisions*. Aerosol Science and Technology, 23:40-50, 1995.

DISTRIBUTION

1	MS0736	Dana A. Powers	6770
1	MS0747	Veena Tikare	6774
1	MS1316	Steven J. Plimpton	1416
1	MS0836	Marcey L. Hoover	1516
1	MS0824	Joel S. Lash	1510
1	MS0899	Technical Library	9536 (electronic)

Sandia National Laboratories